LIMNOLOGY
and
OCEANOGRAPHY

ASLO

Limnol. Oceanogr. 64, 2019, 2172–2186

doi: 10.1002/lno.11177

Weekly dynamics of abundance and size structure of specific nanophytoplankton lineages in coastal waters (Baltic Sea)

Kasia Piwosz *

[1]Center Algatech, Institute of Microbiology Czech Academy of Sciences, Třeboň, Czech Republic
[2]Department of Fisheries Oceanography and Marine Ecology, National Marine Fisheries Research Institute, Gdynia, Poland

Abstract

Nanophytoplankton, the key component of algal communities, remains understudied, thus there is a substantial knowledge gap about dynamics of abundance, biovolume, and cell size of specific algae. Here, I studied weekly changes in abundance, biovolume, cell volume, and cell surface to volume (SV) ratio (> 11,700 cells measured) of specific nanophytoplankton groups using amplicon sequencing and catalyzed reported deposition-fluorescence in situ hybridization. I applied oligonucleotide probes to study major nanophytoplankton groups: chlorophytes, chrysophytes, pelagophytes, cryptophytes, pedinellids, and haptophytes. I designed three novel probes, two for pedinellid species *Apedinella radians* and *Pseudopedinella elastica*, and for a haptophyte genus *Haptolina*. Chlorophytes were the most abundant group, followed by haptophytes and cryptophytes. Abundance and biovolume of specific groups showed distinct seasonal dynamics and fluctuated up to 100-fold within a week. Different groups contributed to nanophytoplankton peaks over the season, and this pattern was consistent down to a genus/species level, as shown for cryptophytes, pedinellids, and haptophytes. Inorganic nutrients were the best explanatory variables for abundance and biovolume, but their importance varied for specific groups. Thus, the differences in seasonal dynamics of different algal groups can be explained by temporal niche separation between them. Changes in nanophytoplankton size structure were substantial, and cell volume varied over 10^4-fold. However, the size dynamics (variability in cell volume and SV ratio) was lower at genus/species level, indicating changes in nanophytoplankton size structure likely resulted from changes in community composition. Temperature and nutrients best explained the size dynamics, but their explanatory power differed for specific nanophytoplankton groups.

Nanophytoplankton (NPP, algae with a cell diameter 2–20 μm) often dominate phytoplankton abundance, biovolume, and production (Piwosz et al. 2015*a*; Roy et al. 2017; Sherr et al. 2007), and its importance may increase with the climate change (Pinckney et al. 2015). Nanoplanktonic algae have higher specific photosynthesis and growth rates than larger or smaller cells (Marañón et al. 2013) and are preferred food for protistan and metazoan grazers (Khanaychenko et al. 2018; Morison and Menden-Deuer 2018). Thus, they are the key component of pelagic food webs and the carbon cycle. However, most NPP species have inconspicuous morphology and cannot be identified using optical microscopy during routine phytoplankton surveys. In result, information on abundance and biovolume of many NPP groups remains accidental. As these values determine productivity and food web structure (Finkel et al. 2010), such knowledge gap limits our understanding of aquatic ecosystems and the accuracy of predictions about community response to natural or anthropogenic impacts.

Rapid development of high throughput sequencing (HTS) methods has allowed for unprecedented insight into diversity of all microorganisms, including algae (Egge et al. 2013; Monchy et al. 2012). In addition to well-known diatoms and dinoflagellates, poorly characterized groups, such as haptophytes, cryptophytes, chrysophytes, and chlorophytes turned out to be important in coastal and open ocean (Balzano et al. 2012; De Vargas et al. 2015; Pinckney et al. 2015; Alves-De-Souza et al. 2017). The occurrence patterns of these groups depend on environmental conditions. For instance, in the brackish Baltic Sea, marine groups, such as coccolitophores, were replaced by freshwater groups, such as synurophytes, along the salinity gradient from about 30 in Kattegat to < 1 in the Bothnian Bay (Hu et al. 2016). Similar changes were observed also at a smaller scale in the estuary of the Vistula River (Gulf of Gdańsk, Baltic Sea; Piwosz et al. 2018). Moreover, high

*Correspondence: piwosz@alga.cz

Additional Supporting Information may be found in the online version of this article.

temporal dynamics of different groups was observed in coastal waters (Egge et al. 2015; Alves-De-Souza et al. 2017).

Unfortunately, HTS methods poorly reflect the abundance of specific groups in original samples (Grujčić et al. 2018; Piwosz et al. 2015*b*), and they do not provide any information on cell morphology, let alone the functional role. For instance, cryptophytes are usually considered autotrophic or mixotrophic (Stefanidou et al. 2018), but uncultured cryptophytes from the basal CRY-1 lineage (Shalchian-Tabrizi et al. 2008) were found to lack chloroplasts (Piwosz et al. 2016) and were subsequently shown to be important bacterivores in freshwaters (Grujčić et al. 2018). Microscopic observations and direct enumeration of specific NPP lineages can be achieved with the use of fluorescence in situ hybridization methods (Lim et al. 1993; Simon et al. 1997, 2000). This technique uses fluorescently labeled oligonucleotide probes that hybridize to ribosomal rRNA in intact cells. The probes are designed based on rRNA gene phylogeny and can target a wide range of taxonomic groups, such as all eukaryotes or phytoplankton classes (Amann et al. 1990; Simon et al. 2000) or a specific genus or lineage (Simon et al. 1997; Piwosz and Pernthaler 2010). The hybridized cells can be visualized using epifluorescent microscopy. It is then possible not only to estimate abundance but also to determine basic morphological features, such as the presence of chloroplasts, shape, and cell size of algae that are indistinguishable using optical microscopy.

Cell size is an important physiological trait that determines metabolic and growth rates of an organism (Finkel et al. 2010; Marañón 2015). Under nutrient limitation, smaller cells have advantage over larger due to the lower overall nutrients requirements and higher surface to volume (SV) ratio: a value that constrains rates of the diffusive flux in nutrient acquisition. Moreover, internal distances are shorter in small cells, facilitating nutrient distribution and processing inside cells (Mei et al. 2009). Finally, cell size and abundance determine the total biovolume of algae and thus their importance in the carbon cycle. However, in situ dynamics of NPP size–structure, both general and for specific algal groups, remains unknown. Consequently, it is still to be explored whether cell size and abundance of an algal species response similarly to environmental change.

The aim of this study was to reveal temporal dynamics of abundance, biovolume, cell volume, and cell SV ratio of total NPP and of specific algal groups in coastal waters of the Gulf of Gdańk (Baltic Sea) and to link their dynamics to changes in the environmental conditions. The focal groups, studied by catalyzed reported deposition-fluorescence in situ hybridization (CARD-FISH), were chlorophytes, cryptophytes (including lineage CRY-1), pedinellids (including species *Apedinella radians* and *Pseudopedinella elastica*), haptophytes (including Pavlovophyceae and genera *Prymnesium*, *Haptolina,* and *Chrysochromulina*), chrysophytes, and pelagophytes. They were selected based on pyrosequencing of weekly collected samples and on the previous study in the region (Piwosz et al. 2018). I hypothesized that (1) different algal groups would contribute to NPP maxima during the season, (2) their cell volume and cell SV ratio would vary over the season, and (3) abundance, biovolume, cell volume, and cell SV ratio of different NPP groups would correlate differently with the environmental variables, which together would suggest temporal niche separation between the studied groups. I also expected that abundance and biovolume would be more explained by the temperature, whereas cell volume and cell SV ratio by concentrations of inorganic nutrients.

Material and methods

Sampling

Surface water samples were collected weekly from 12 April to 07 November 2012 from a coastal station (54°31′05.2″N 18°33′21.5″E) in the Gulf of Gdansk (southern Baltic Sea, Poland). Ten liters of water was prefiltered through a 20-μm-mesh phytoplankton net into a plastic container that had been cleaned with 10% HCl, thoroughly rinsed with deionized water, and rinsed three times with the sampled water on site. The collected water was transported to the laboratory within 15 min. Temperature and salinity were measured in situ with a CC-411 conductivity meter (Elmetron Sp.j).

DNA extraction and sequencing

About 0.8–2.5 liters of water was filtered onto a polyethersulfone filter (GPWP, diameter 47 mm, pore size 0.22 μm, Merck KGaA) under sterile conditions. 4.6 liters was filtered on the 07 November. DNA was extracted using PowerWater DNA isolation kit (MO BIO Laboratories). The V4 fragment of 18S rRNA genes was amplified with TAReuk454FWD1 (5′-CCAG CASCYGCGGTAATTCC-3′) and TAReukREV3 (5′-ACTTTCGTT CTTGATYRA-3′) primers using polymerase chain reaction conditions as described by Stoeck et al. (2010), and sequenced on 454 platform by Research and Testing laboratories. As the reverse primer TAReukREV3 poorly targets haptophytes, we additionally sequenced samples with high haptophyte abundance (23 May–30 July) using the reverse primer HaptoR1 (5′-CGAAACCAA CAAAATAGCAC-3′; Egge et al. 2013).

Sequence analysis

Raw sequencing data included 328,505 reads (3911–26,848 per sample) of length ranging from 221 to 581 bp. They were analyzed by a custom-made pipeline at the Limnological Station, University of Zurich, as described before (Shabarova et al. 2014). Raw sff flowgrams were denoised using AmpliconNoise (Quince et al. 2011). After quality filtering (bases with Phred score < 30 were trimmed), sequences were trimmed to 250 bp, and chimeric sequences were discarded with UCHIME (Edgar et al. 2011). These procedures reduced the dataset to 146,552 sequences (from 1707 to 15,233 per sample). Operational Taxonomic Unit (OTUs) were clustered by average linkage at similarity levels of 97% upon the pairwise alignment by the Needleman–Wunsch algorithm. The most closely related sequence for each OTU was identified using pairwise alignment

to the PR2 reference data (Guillou et al. 2013), and the corresponding taxonomic information toghether with the similarity to the query sequence were assigned. The same procedure was used to analyze haptophyte data. The sequences obtained using the general eukaryotic primers set are available under Bioproject accession number PRJEB23971, and using the reverse haptophyte primer under Bioproject accession number PRJEB31858.

Sequence data were further analyzed in the R environment (R Core Team 2015) and Bioconductor. Diversity indexes were calculated in the SpadeR package (Chao et al. 2015) on samples rarefied to 1700 reads using the physeq package (Mcmurdie and Holmes 2013). Rarefactions curves were prepared using the vegan package (Oksanen et al. 2018) and Figs. 1–5 were prepared using functions from packages physeq, ggplot2 (Wickham 2009), and cowplot (Wilke 2018).

Design of oligonucleotide probes

I designed three oligonucleotide probes: two for pedinellids species *A. radians* and *P. elastica* and for a haptophyte genus *Haptolina*. Phylogenetic trees were calculated in the ARB software (Ludwig et al. 2004) using almost full-length rRNA gene sequences available in the 115 release of the SSURef SILVA database. The alignments were manually improved prior to the analysis. The phylogenetic tree of Prymnesiophyceae was calculated for 164 sequences with 1903 positions filtered by maximum frequency > 50% and Pavlovophyceae as on outgroup. For Pedinellales, the phylogenetic tree was calculated using 35 sequences and 1746 position (maximum frequency > 50%) and sequences from *Dictyocha* spp. as an outgroup. Hundred bootstrapped maximum likelihood trees were calculated for each group, using the RAxML algorithm and gamma model for base substitution (Stamatakis et al. 2008). New oligonucleotide probes were designed with the ARB's Probe Design module. The specificity of the probes was tested in silico using the ARB Probe_Match function and the SILVA online ProbeCheck tool against the ENA database (EMBL-EBI, accessed on 28 January 2019). Theoretical hybridization conditions were evaluated with the mathFISH on-line tool (Yilmaz et al. 2011) and optimized on environmental samples hybridized at increasingly stringent conditions (20–60% of formamide concentration, 10% steps; Massana et al. 2006) and the highest formamide concentration at which the brightness of hybridized cells was still unaffected, was chosen (Table 1). Probes for *A. radians* were also tested against nontarget *Pseudopedinella* sp. RCC668 strain and probe for *Haptolina* against nontarget *Prymnesium parvum* RCC2056 and *Chrysochromulina leadbeaterii* RCC3424 strains.

Total nanoplankton counts

About 20 mL of the sample was fixed using the Lugol–formalin–$Na_2S_2O_3$ method (Sherr et al. 1987) and filtered on polycarbonate membrane filter (pore size 0.8 μm, diameter 25 mm, Cyclopore, Whatmann). Filters were air dried, stained with 4′-6-diamidino-2-phenylindole (DAPI; 1 μg mL^{-1}; Coleman 1980) and mounted in antifading glycerol medium (Citifluor AF1 and Vectashield, v/v = 5 : 1). At least 200 flagellates were counted in 10 randomly selected microscopic fields of view at 1000X magnification by epifluorescence microscopy (AxioImager.M1, Carl Zeiss).

Catalyzed reported deposition-fluorescence in situ hybridization

About 200 mL of water was fixed as described for the total nanoplankton (TNP) counts. They were filtered onto white polycarbonate filters (diameter 47 mm, pore size 0.8 μm, Cyclopore, Whatmann), which were then air dried and stored at −20°C.

The CARD-FISH procedure was performed as described in Piwosz and Pernthaler (2010). The filters were embedded in 0.1% (w/v) agarose and incubated in 0.1 mol L^{-1} HCl for 20 min at room temperature. Subsequently, they were cut into 20 sections with an approximate surface of 87 mm^2. Hybridization was performed at 35 or 46°C with horseradish peroxidase-labeled oligonucleotide probes (Biomers, final concentration: 0.5 ng μL^{-1}). I used 14 probes, details on them and the hybridization conditions are given in Table 1. Filter sections were washed for 30 min at 2°C warmer conditions than the hybridization temperature, and then equilibrated in 1 × PBS-T (1 × PBS + 0.01% [v/v] Triton-X) for 45 min at 37°C. Fluorescent signal from Alexa488-labeled tyramides (Molecular Probes, Invitrogen) was amplified at 37°C for 30 min. Hybridized filter sections were mounted on microscope slides with antifading glycerol medium (Citifluor AF1 : Vectashield, v/v = 5 : 1 with 1 μg mL^{-1} of DAPI) and stored at −20°C.

CARD-FISH preparations were analyzed by epifluorescence microscopy at 1000X magnification (AxioVision.M1, CarlZeiss). Microphotographs from 10 to 20 randomly selected fields of view were obtained using ultraviolet/blue (excitation/emission) for DAPI signals, blue/green for Alexa488 signal from the hybridized cells, and green/red for chloroplasts autofluorescence. The micrographs were analyzed manually in the ZEN software (Carl Zeiss Microimaging). All visualized DAPI-stained (min. 1000) and hybridized cells were counted. NPP cells were counted as Euk516-hybridized cells of appropriate size showing chloroplast autofluorescence. Abundance of each group was calculated from proportions of CARD-FISH counts to TNP counts by DAPI.

Length and width of the hybridized cells were measured using the length tool in Zen, and their volume and surface were calculated assuming cell shape to be a prolate spheroid (Eqs. 1, 2; Olenina et al. 2006). When possible, 100 cells per sample were measured, otherwise all hybridized cells were measured (Table 1). More than 11,700 cells were measured in total. Biovolume (in μm^3 mL^{-1}) was calculated by multiplying average cell volume by cell abundance.

Volume of prolate spheroid:

$$\frac{\pi}{6} \times a^2 \times c \quad (1)$$

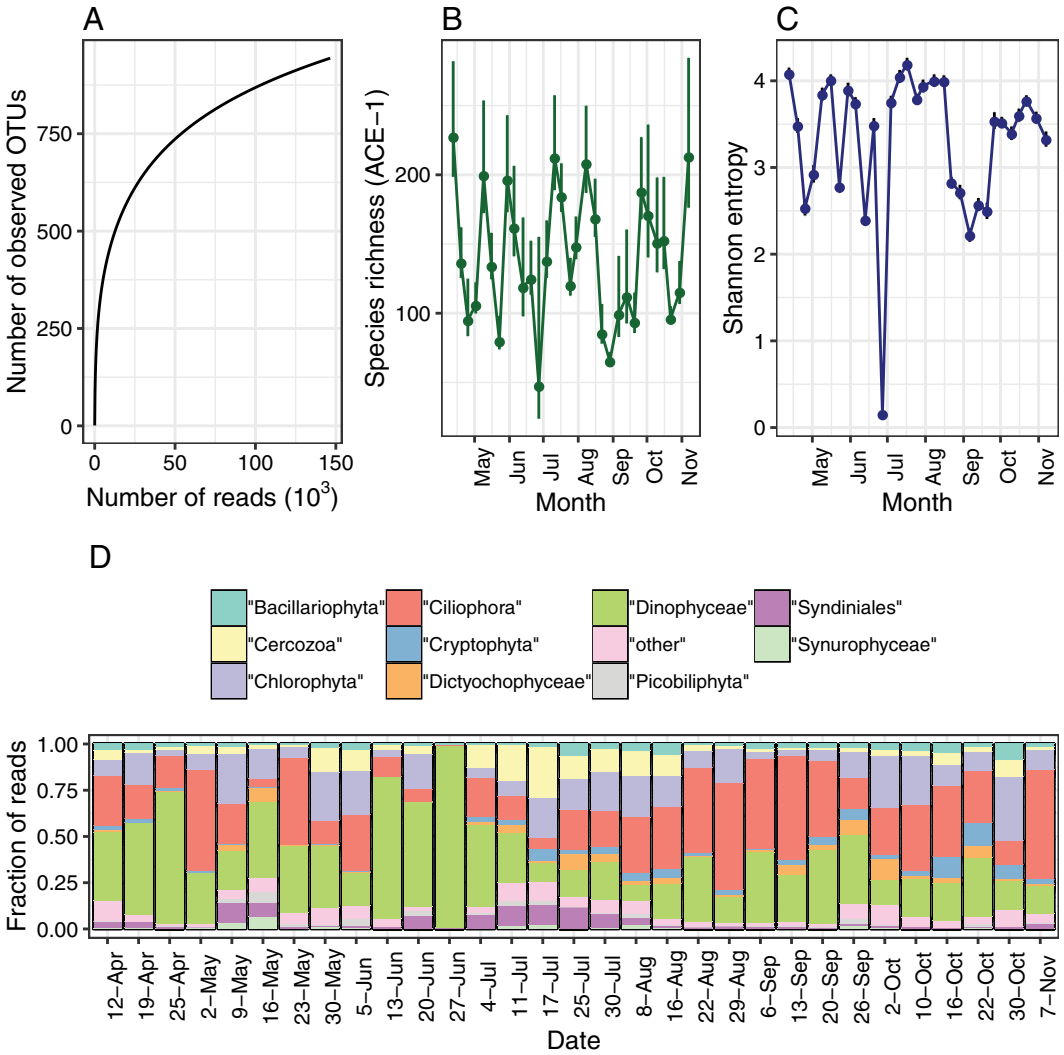

Fig. 1. Nanoplankon diversity in the Gulf of Gdansk in 2012 (based on pyrosequencing data). (**A**) Rarefaction curve for the whole dataset (separate rarefaction curves for each sample are available in Supporting Information Fig. S1); (**B**) estimated species richness in the samples; (**C**) estimated Shannon entropy index in the samples; (**D**) fraction of reads in samples coming from different phylogenetic groups at division (Cercozoa, Chlorophyta, Ciliophora, Cryptophyta, and Picobiliphyta) or class (Bacillariophyta, Dictyochophyceae, Dinophyceae, Syndiniales, and Synurophyceae) level; error bars represent 95% confidence intervals in panels **B** and **C**.

Surface of prolate spheroid:

$$2\pi a^2\left(1+\frac{c}{ae}\times\arcsin e\right);\quad \text{where } e=\sqrt[2]{1-\frac{a^2}{c^2}} \qquad (2)$$

where a is cell width and c is cell length ($a < c$).

Chlorophyll *a* (fraction < 20 μm)

About 50–100 mL of sampled water was filtered onto glass-fiber GF/F filters (Whatmann). The filters were stored in the dark at −20°C and analyzed within 1 month of collection. Chlorophyll *a* (Chl *a*) was extracted for 24 h in 90% acetone in the dark at 4°C and measured using fluorometric method (Evans et al. 1987) with a Turner Designs 10-005R fluorometer.

Nutrients

About 500 mL of water was collected in an acid-clean container, frozen at −20°C and analyzed within a month. Concentrations of N-NO_3, N-NO_2, and N-NH_4 (their sum is referred to as dissolved inorganic nitrogen [DIN]), soluble reactive phosphorous (SRP), and dissolved silicate (DSi) were determined by methods recommended for the Baltic Sea (Grasshoff et al. 1976). The detection limits for N-NO_3 was 0.1 μmol L^{-1}; for N-NO_2 was 0.02 μmol L^{-1}; for N-NH_4 was 0.05 μmol L^{-1}; for SRP was 0.01 μmol L^{-1}; and for DSi was 0.1 μmol L^{-1}.

Statistical analyses

The relationships between environmental data and the abundance, biovolume, cell volume, and cell SV ratio of

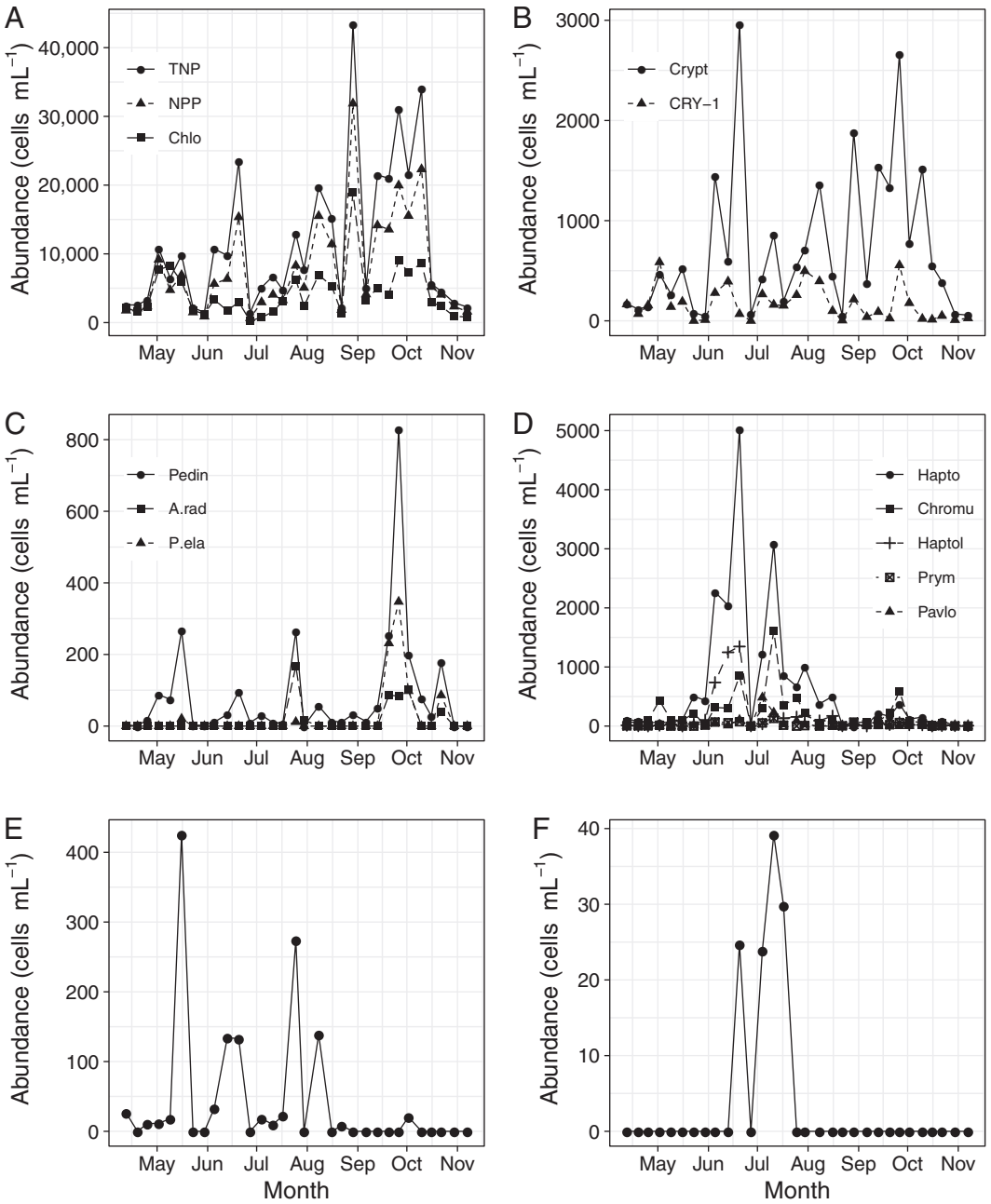

Fig. 2. Weekly abundances of studied nanoplankon groups in the Gulf of Gdansk in 2012 (based on CARD-FISH data). (**A**) TNP (phototrophic and heterotrophic), NPP, and chlorophytes (Chlo); (**B**) cryptophytes (Crypt) and CRY-1 lineage (CRY-1); (**C**) pedinellids (Ped), *A. radians* (A.rad) and *P. elastica* (P.ela); (**D**) haptophytes (Hapto), *Chrysochromulina* (Chromu), *Haptolina* (Haptol), *Prymnesium* (Prym), and pavlovophytes (Pavlo); (**E**) plastidic chrysophytes; (**F**) pelagophytes. Scale on Y axes differs between the panels.

studied groups (derived from microscopic analysis as described above) were analyzed by Bray–Curtis dissimilarity distance-based linear models (DistML) and distance-based redundancy analysis (dbRDA) in the PERMANOVA+ add-on package of the PRIMER7 software (Primer). Environmental variables were normalized, and a correlation matrix for the whole set was calculated. From the variables that were strongly correlated (absolute value of the correlation coefficient > 0.7) only one was chosen for further analysis. Abundance and biovolume were $\log_{10}(X + 1)$ transformed. Cell volume and SV ratio data were lognormally distributed, thus were $\log_e(X)$ transformed for statistical analysis and graphical representation. Analysis was performed using a step-wise selection procedure, and the best model was selected based on the statistical significance (9999 permutations), and the values of the Akaike's information criterion and the Bayesian information criterion (Anderson and Legendre 1999; Legendre and Anderson 1999). DistML

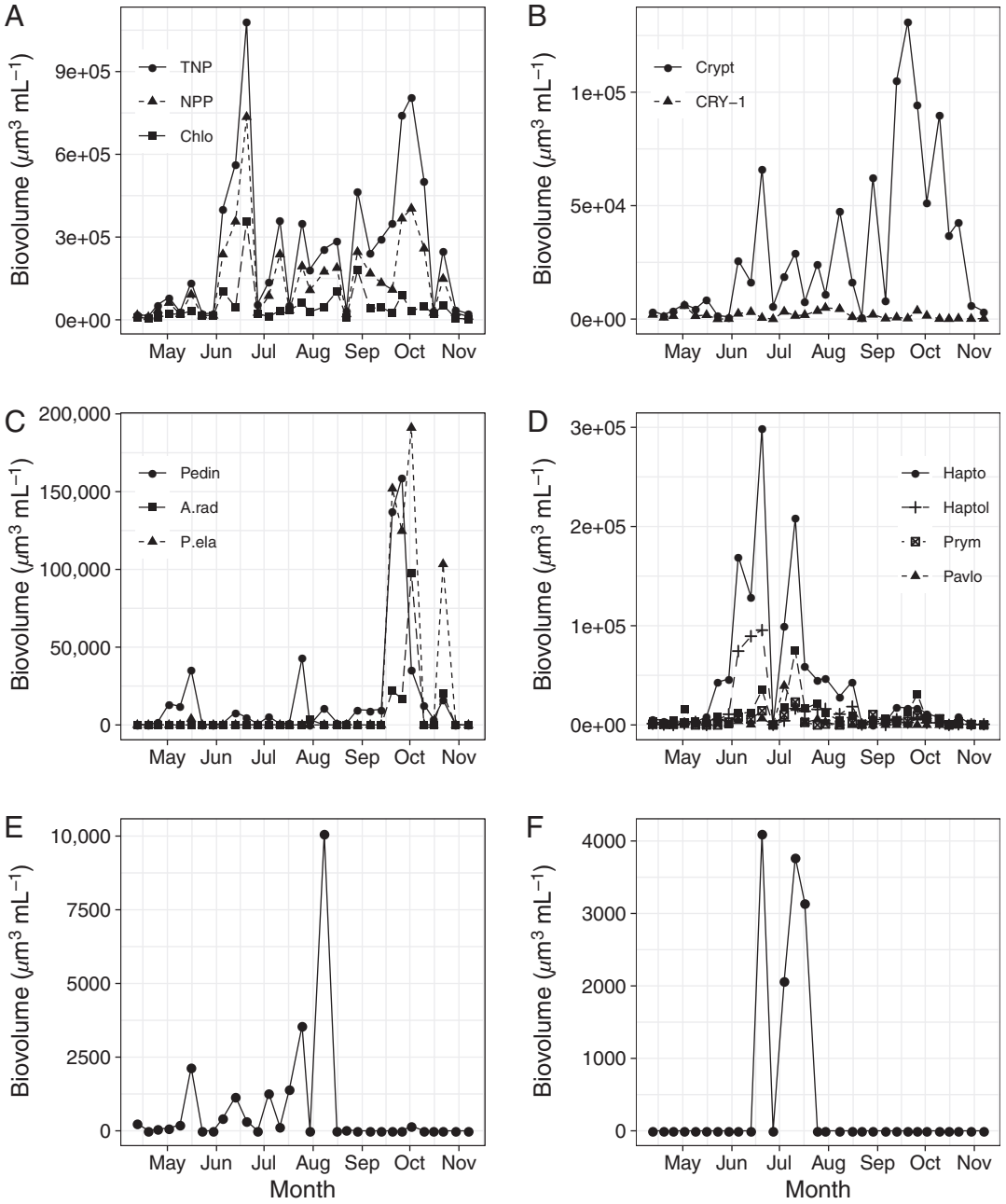

Fig. 3. Weekly biovolumes of studied nanoplankon in the Gulf of Gdansk in 2012 (based on CARD-FISH data). (**A**) TNP (phototrophic and heterotrophic), NPP, and chlorophytes (Chlo); (**B**) cryptophytes (Crypt) and CRY-1 lineage (CRY-1); (**C**) pedinellids (Ped), *A. radians* (A.rad), and *P. elastica* (P.ela); (**D**) haptophytes (Hapto), *Chrysochromulina* (Chromu), *Haptolina* (Haptol), *Prymnesium* (Prym), and pavlovophytes (Pavlo); (**E**) Plastidic chrysophytes; (**F**) Pelagophytes. Scale on Y axes differs between the panels.

and dbRDA analyses for cell volume and cell SV were additionally performed upon excluding groups that were too infrequent to provide enough specimen for measurements in at least four samples (plastidic chrysophytes, pelagophytes, *A. radians*, *P. elastica, Haptolina, Prymnesium*, and pavlovophytes). As the results did not differ substantially, only the analysis for the whole data set is presented and discussed here.

Results

Diversity of picoplankton and nanoplankton in the Gulf of Gdańsk by amplicon sequencing

Due to the use of general eukaryotic primers and collection of organisms onto 0.22 μm filters, diversity of both picoplankton and nanoplankton and of phototrophs and heterotrophs was investigated here. The total number of all picoplankton and

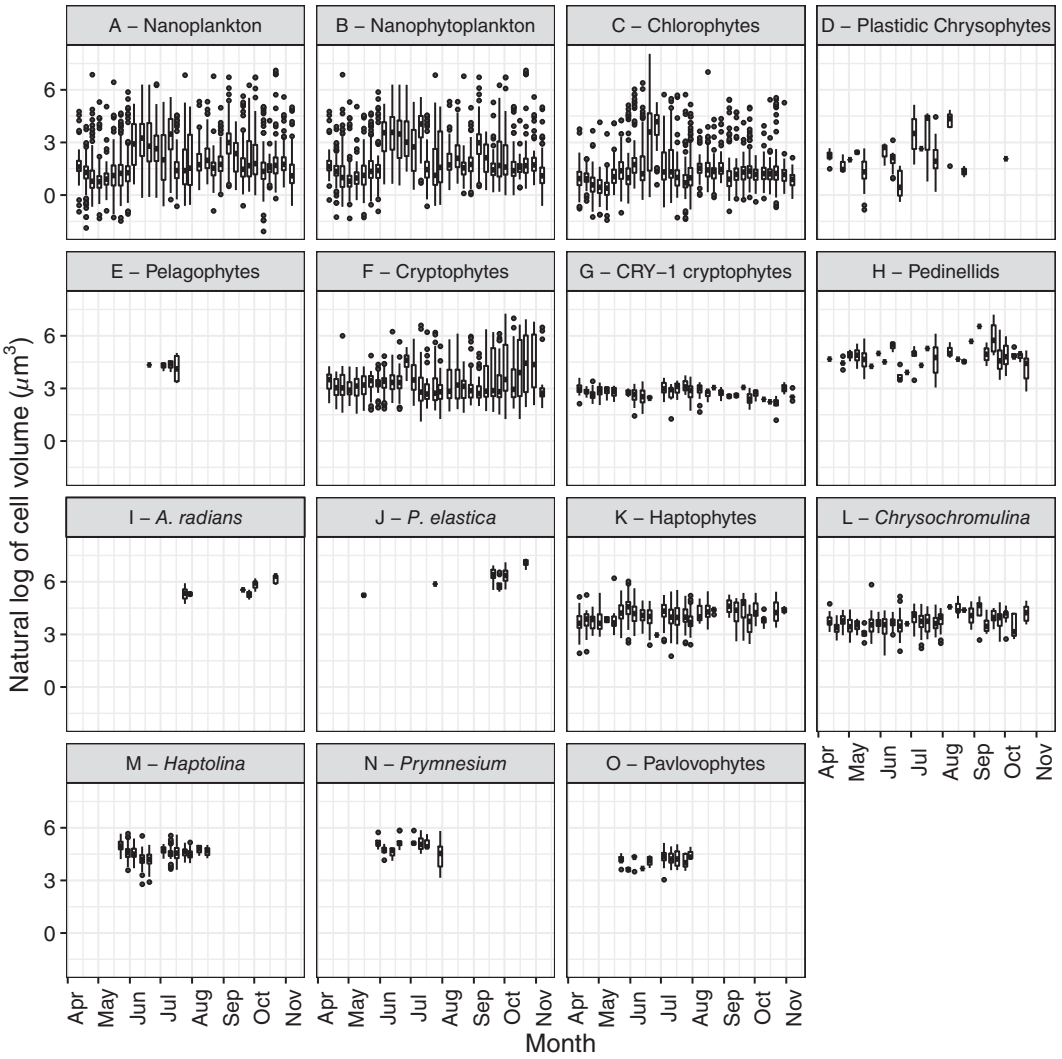

Fig. 4. Cell volumes of studied nanoplankon groups in the Gulf of Gdansk in 2012. Due to the lognormal distribution, the values were transformed using natural logarithm. (**A**) Total (photo- and heterotrophic) nanoplankton (TNP); (**B**) nanophytoplankton (NPP); (**C**) chlorophytes; (**D**) plastidic chrysophytes; (**E**) pelagophytes; (**F**) cryptophytes; (**G**) CRY-1 lineage; (**H**) pedinellids; (**I**) *Apedinella radians*; (**J**) *Pseudopedinella elastica*; (**K**) haptophytes; (**L**) *Chrysochromulina*; (**M**) *Haptolina*; (**N**) *Prymnesium*; (**O**) pavlovophytes.

nanoplankton OTUs was 945. The rarefaction curve for the whole sampling season (Fig. 1A) as well as curves for the individual samples (Supporting Information Fig. S1) just started to bend, indicating that the diversity was not exhaustively sampled even during such high-frequency–sampling campaign. The estimated number of phylotypes in one sample ranged from 24 to 155 on 27 June to 198–282 on 12 April (Fig. 1B). The changes in alpha diversity were very dynamic. The longer period of higher diversity was observed in July and August, and it was followed by the period of lower diversity until mid-September (Fig. 1C). The lowest diversity was on 27 June, during bloom of a dinoflagellate *Heterocapsa triquetra*, whose sequences contributed in almost 98% to all reads on that day (Fig. 1D; Supporting Information Table S1). Such high dynamics of alpha diversity emphasizes the need of considering frequent sampling in studies of microbial diversity.

As the focus of my study was on NPP, I assigned specific OTUs into possible groups of interest to be further studied by CARD-FISH (Supporting Information Table S1). Heterotrophic organisms, such as ciliates, cercozoa, and syndiniales, were excluded. A high proportion of reads was affiliated with dinoflagellates (Fig. 1D), most of which could not be assigned below the class level. Those that were belonged either to larger species, such as *Gymnodinium catenatum* or *H. triquetra*, or to nonphototrophic species, such as *Gyrodinium dominans*. Therefore, dinoflagellates were also not further investigated. About 142 OTUs (15%) were tentatively assigned to NPP, and they contributed above 18% of all reads (Supporting Information Table S1). In addition, 45 OTUs affiliated with Chrysophyceae–Synurophyceae remained unassigned, but they contributed only < 1% to the total number of reads.

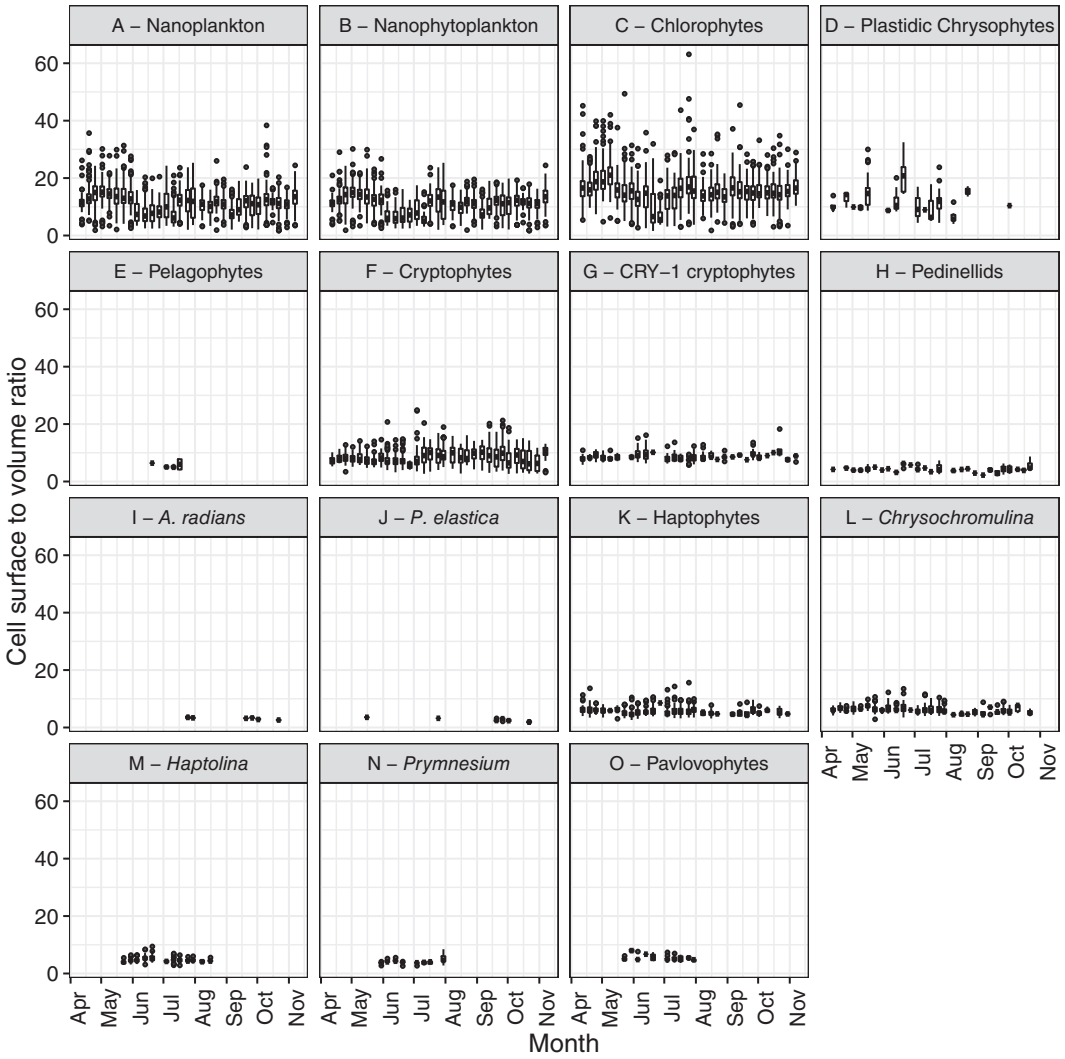

Fig. 5. Cell SV ratios of studied nanoplankon groups in the Gulf of Gdansk in 2012. (**A**) Total (photo- and heterotrophic) nanoplankton (TNP); (**B**) nanophytoplankton (NPP); (**C**) chlorophytes; (**D**) plastidic chrysophytes; (**E**) pelagophytes; (**F**) cryptophytes; (**G**) CRY-1 lineage; (**H**) pedinellids; (**I**) *Apedinella radians*; (**J**) *Pseudopedinella elastica*; (**K**) haptophytes; (**L**) *Chrysochromulina*; (**M**) *Haptolina*; (**N**) *Prymnesium*; (**O**) pavlovophytes.

The highest proportion of reads originating from plausibly nanophytoplanktonic groups belonged to chlorophytes (Fig. 1D) and affiliated with species and genera such as *Oocystis marssonii*, *Scenedesmus abundans*, and *Chlamydomonas hedleyi* (Supporting Information Table S1). However, picoplanktonic genera and species, such as *Micromonas* sp. Clade-B.E.3, *Bathycoccus prasinos*, *Chlorella* sp., or *Nannochloris* sp., were also present. Cryptophytes' sequences were most represented in libraries starting from July (Fig. 1D), and they originated from basal CRY-1 lineage and genera *Teleaulax* and *Geminigera*. Dictyochophyceae, mainly pedinellids, made up larger proportion of reads in July/August and September (Fig. 1D). Contribution of sequences originating from haptophytes was low due to the reverse primer mismatch, so they were additionally sequenced with a specific haptophyte primer (Supporting Information Table S2). Three most abundant genera, which together contributed to almost 68% of all haptophyte reads, where *Prymnesium* (28.7%), *Haptolina* (22.5%), and *Chrysochromulina* (14.4%).

The sequencing data served mainly as the base to choose algal groups for analysis of their temporal dynamics of abundance and cell size using CARD-FISH (Table 1).

Probes design and validation

I designed and validated three oligonucleotide probes: Aperad631, Pseela1352, and Haptol640, for *A. radians*, *P. elastica*, and *Haptolina* spp., respectively (Table 1). Cells hybridized with the new probes are shown in Supporting Information Fig. S2.

The pedinellids tree was well resolved (Supporting Information Fig. S3A; Sekiguchi et al. 2003). Probe Aperad631 targets only a sequence of *A. radians* and 100% identical environmental sequence KP404871, and it has at least three mismatches to any other sequence available in the SILVA database. This probe was tested

Table 1. List of probes used in this study. HB (%), concentration of formamide in the hybridization buffer; *T*, hybridization temperature (washing temperature was 2°C higher); N_t, total number of measured cells; and N_m, mean, minimal, and maximal (in the parentheses) number of cells measured per sample.

Probe name	Target group	Sequence (5′ → 3′)	HB (%)	*T* (°C)	Reference	N_t	N_m
Euk516	All eukaryotes	ACC AGA CTT GCC CTC C	20	35	Amann et al. (1990)	3160	101.9 (100–132)
Euk516*	NPP	ACC AGA CTT GCC CTC C	20	35	Amann et al. (1990)	2504	80.7 (50–106)
Chlo02	Chlorophyta	CTT CGA GCC CCC AAC TTT	40	35	Simon et al. (2000)	3481	112.3 (30–270)
Chry1037	Plastid of chrysophytes	GCA CCA CCT GTG TAA GAG	20	35	Fuller et al. (2006)	120	8.0 (1–44)
Pela01	Pelagophyceae	ACG TCC TTG TTC GAC GCT	40	35	Simon et al. (2000)	13	3.3 (1–4)
CryptB	Cryptophyceae	ACG GCC CCA ACT GTC CCT	50	46	Metfies and Medlin (2007)	1591	51.3 (4–104)
CryptP_680	CRY1 cryptophytes	CAC AGT AAA CGA TCC GCG CAA	40	35	Piwosz et al. (2016)	336	11.6 (1–50)
Ped675	Pedinellales	TCA CAG TAA ACG ACA GGC GT	45	35	Piwosz and Pernthaler (2010)	185	6.9 (1–29)
Aperad631	*A. radians*	CCA GCA TGA GTC CCC CTG AGG	45	46	This study	45	7.5 (2–14)
Pseela1352	*P. elastica*	GCG AAG CAT TCC CAG CAC TAT	30	46	This study	52	8.7 (1–19)
Prym02	Haptophyta	GGA ATA CGA GTG CCC CTG AC	40	35	Simon et al. (2000)	1343	48.0 (1–169)
ChrysB2-Clade02	*Chrysochromulina*	AGT CGG GTC TTC CTG CAT GT	40	46	Simon et al. (1997)	634	23.1 (1–103)
PrymB1-Clade01	*Prymnesium*	GGA CTT CCG CCG ATC CCT AGT	50	46	Simon et al. (1997)	75	10.0 (5–20)
Haptol640	*Haptolina*	GGC AGA CCG GCA GGC AGG CCC	60	35	This study	568	47.3 (4–113)
Pavlova01	Pavlovophyceae	CAC CTC TCT CTA CGG AAT	30	35	Eller et al. (2007)	99	9.9 (1–43)

*For NPP counts, only Euk516 hybridized cells showing chlorophyll autofluorescence were included.

against a culture of nontarget species *Pseudopedinella* sp. RCC668 (88% identity) and it did not show positive signal (Supporting Information Fig. S2). Probe Pseela1352 targets two sequences that cluster together with 100% bootstrap support (Supporting Information Fig. S3A) and an environmental sequence KP404878 that is 100% identical to sequence of *P. elastica*, and it does not target a sister clade, to which some other *Pseudopedinella* species belong. I did not have a culture on which I could test the probe, but it has at least four mismatches to any other sequences, so it is unlikely it would hybridized to untargeted species.

Probe Haptol640 targets all cultured *Haptolina* species that form a monophyletic clade with 85% bootstrap support (Supporting Information Fig. S3B) and four other sequences with 99% identity to *Haptolina hirta*. The probe has at least two mismatches to untargeted sequences. The probe does not target the sequence AM490995 that originate from an organisms classified as *Haptolina brevifila* strain Kawachi (Medlin et al. 2008). This is not the original strain that has been used in a study establishing genus *Haptolina* (Edvardsen et al. 2011), and it clusters with *Chrysochromulina parkeae* and *Braarudosphaera bigelowii* with 85% bootstrap support (Supporting Information Fig. S3B). This sequence has 99% identity to sequence AB058358, classified as *Chrysochromulina brevifilum* strain MBIC10518, which also clusters with *C. parkeae* in Edvardsen et al. (2011). Thus, it is likely that sequence AM490995 does not originate from a *Haptolina* species. The probe was tested against nontarget species *P. parvum* RCC2056 and *C. leadbeaterii* RCC3424, and it did not show positive signal, which confirms its specificity (Supporting Information Fig. S2).

Abundance and biovolume dynamics of NPP using CARD-FISH

NPP contributed 45% to 92% to the TNP abundance (Fig. 2A). Its dynamics was very high, with up to 30-fold changes between the weeks. NPP abundance varied from 0.6 to 38.9×10^3 cells mL^{-1} and was the highest in September and October and the lowest on 27 June (Fig. 2A), during a massive bloom of a dinoflagellate *H. triquetra* (5.3×10^6 cells L^{-1}, Chl *a* concentration 25.6 $\mu g\ L^{-1}$; Supporting Information Fig. S4). Specific algal groups showed distinct abundance dynamics, and NPP peaks consisted of different algae: chlorophytes showed maxima in September (Fig. 2A), cryptophytes in June and October (Fig. 2B), pedinellids in October (Fig. 2C), haptophytes in June–July (Fig. 2D), plastidic chrysophytes in May (Fig. 2D), and pelagophytes in June–July (Fig. 2E). Abundance of these algal groups changed up to 300 times between the weeks. I could show for cryptophytes, pedinellids, and haptopytes that their maxima were also formed by different species or genera. For instance, cryptophyceaen abundance in April and May was dominated by basal cryptophytes from a heterotrophic CRY-1 lineages, whose contribution to June and September peaks was substantially lower (Fig. 2B). Similarly, the pedinellid peak in August was formed mainly by *A. radians*, whereas the peak in October was formed mainly by *P. elastica* with smaller contribution of *A. radians* and other pedinellids (Fig. 2C). Finally, *Chrysochromulina* and *Haptolina* contributed most to the haptophyte peak in June, whereas the peak in July consisted mainly of *Chrysochromulina* with only minor contribution from *Prymnesium* and Pavlovophyceae (Fig. 2D). This pattern, consistently found for different NPP classes and orders, indicates

possibility of temporal niche separation not only between distant groups but also between closely related species and genera.

The biovolume generally followed the pattern observed for the abundance, but its maxima were shifted for some groups (Fig. 3). For example, biovolume of all nanoplankton, NPP, and chlorophytes peaked in June (Fig. 3A) rather than in autumn months like observed for the abundance, whereas biovolume of cryptophytes (Fig. 3B) and plastidic chrysophytes (Fig. 3E) peaked in autumn rather than in spring. In general, the observed dynamics in biovolume also supports the hypothesis that different algal groups contributed to NPP peaks during the season.

HTS and microscopic analysis showed different composition of nanoplankton community (Figs. 1–2). For instance, HTS data indicated importance of dinoflagellates and ciliates in nanoplankton, which together contributed 65% of all reads (37.2% and 27.8%, respectively; Supporting Information Table S1.). In contrast, microscopic data pointed to dominance of chlorophytes, which contributed from 13% to almost 100% of TNP abundance (47% on average). Similar disagreement was also present for haptophyte data, for which HTS data for samples collected from 23 May to 30 July pointed to *Prymnesium* to be the dominant genus at that time (28.7% of total reads; Supporting Information Table S2), whereas it contributed below 4% to haptophyte abundance estimated by CARD-FISH (Fig. 2D). Due to this disagreement, I decided to focus on data obtained only from microscopic measurements.

Dynamics of nanoplankton cells' volume and surface-to-volume ratios

All groups studied by CARD-FISH were predominantly nanoplanktonic (cell size between 2 and 20 μm). NPP cell volume ranged over four orders of magnitude: from 0.3 to 3140.35 μm^3 and showed log normal distribution for all studied groups (Supporting Information Fig. S5). The average cell volume changed very rapidly from 1 week to another (Fig. 4). The largest cells were observed in June, at the beginning of September, and in October and the smallest in spring (Fig. 4A,B). Chlorophytes were generally the smallest, with mean cell volume around 10 μm^3 most of the season. Interestingly, small chlorophytes almost entirely disappeared during the bloom of *H. triquetra* on June 27, and the average cell volume increased to 98.95 $\pm$ 318.84 μm^3 at that time, with the largest cells being > 3000 μm^3 (Fig. 4C). Plastidic chrysophytes were also rather small, and their cell volume was < 13 μm^3 except for mid-July and early August, when it was > 60 μm^3 (Fig. 4D). The average cell volume of pelagophytes was 78.16 $\pm$ 34.42 μm^3 (Fig. 4E). Cell volumes of cryptophytes were low in spring and gradually increased after summer, when large, photrophic cells dominated (Fig. 4F). Their small mean cell volume in early spring was caused by the high contribution of CRY-1 lineage, the cell volume of which was generally invariable over the season (Fig. 4G). The mean cell volume of pedinellids was 156.26 $\pm$ 170.13 μm^3 (Fig. 4H), and it ranged from 16.86 to 1347.32 μm^3. *P. elastica* was larger than *A. radians* (Fig. 4I,J). Haptophyte cell volume ranged from 5.97 to 507.94 μm^3, but the mean did not vary much over the sampling season (Fig. 4K). *Chrysochromulina* was the smallest (from 6.03 to 351.33 μm^3, mean 46.35 $\pm$ 27.79 μm^3), followed by *Haptolina* (from 16.59 to 296.77 μm^3, mean 92.18 $\pm$ 40.52 μm^3) and *Prymnesium* (from 23.32 to 354.59 μm^3, mean 154.24 $\pm$ 71.55 μm^3). The cell volume of *Chrysochromulina* slightly increased in autumn (Fig. 4L), but cell volume of *Haptolina* and *Prymnesium* did not vary (Fig. 4M,N). Cell volume of pavlovophytes ranged from 21.44 to 170.07 μm^3 (Fig. 4O).

Cell SV ratio varied from 1.6 to 63.3 and showed log normal distribution for all studied groups (Supporting Information Fig. S6). Its seasonal dynamics showed opposite trends to those observed for cell volume. The highest SV ratios were observed in April and May, and the lowest in summer for all nanoplankton, NPP and chlorophytes (Fig. 5A–C). SV ratios for other groups varied only slightly and without a clear seasonal pattern (Fig. 5D–O). A general pattern that emerged here was that the variability of cell volume and SV ratio tend to be lower for specific groups, indicating that the changes in size structure within NPP may be related to changes in community composition rather than to physiological responses of algal species.

Correlations with environmental variables

The dynamics of the environmental variables was typical for the area, with maximal temperatures and minimal nutrient concentrations in summer (Supporting Information Fig. S4). Interestingly, there was a sudden peak of SRP concentration accompanied by a massive bloom of a dinoflagellate *H. triquetra* on 27 June, which coincided with very low nanoplankton diversity, abundance, and biovolume (Figs. 1–3).

The measured characteristics of studied NPP groups correlated differently with the environmental variables. Dynamics of abundance and biovolume (obtained using CARD-FISH) were best explained by temperature, DIN, SRP, and DSi, which explained 41.5% of total variance in abundance ($p = 0.0129$) and 38.7% ($p = 0.0145$) in biovolume (Fig. 6A,B). DIN was negatively related with most groups, explaining 16.8% of variance in abundance and 15.2% in biovolume, whereas temperature, SRP, and DSi explained about 7–8% each. Cell volume also significantly correlated with temperature, DIN, and SRP, which together explained 48.5% of its total variance ($p = 0.0014$; Fig. 6C), but most of the variance (21%) was explained by temperature, with DIN and SRP accounting for about 13–14% of the explained variance each. Similarly, temperature, DIN, and SRP collectively explained 42.7% of the total variance is the SV ratios ($p = 0.0118$; Fig. 6D), but it was SRP that was most important (22.4%). These correlative analyses disagree with my initial assumption that abundance and biovolume will be more explained by the temperature, while cell volume and SV ratio by concentrations of inorganic nutrients. Nevertheless, abundance, biovolume, cell volume, and SV ratio of different NPP groups did correlate differently with the environmental variables, suggesting that the environmental factors that well explain total NPP variability may be of lower importance for specific groups (Fig. 6; Supporting Information Table S3). For

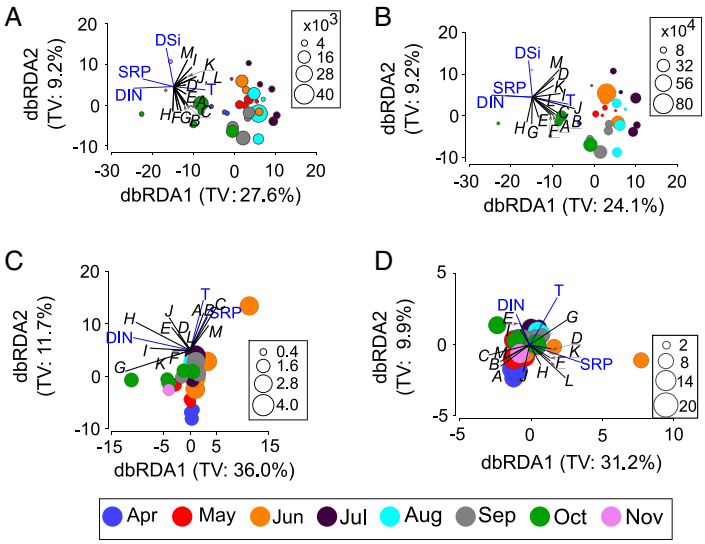

Fig. 6. Ordination plots of dbRDA relating the observed variability in abundance (**A**), biovolume (**B**), cell size (**C**), and cell SV ratio (**D**) of NPP groups (black lines) to environmental variables (blue lines, only statistically significant variables are shown). NPP groups are coded by letters: A, TNP; B, NPP; C, chlorophytes; D, plastidic chrysophytes; E, cryptophytes; F, pedinellids; G, *A. radians*; H, *P. elastica*; I, haptophytes; J, *Chrysochromulina*; K, *Haptolina*; L, *Prymnesium*; and M, pavlovophytes. Size of the circles corresponds to abundance of NPP in cells mL^{-1} (panel **A**), biovolume of NPP in μm^3 mL^{-1} (panel **B**), average cells volume (transformed by natural logarithm) of NPP in μm^3 (panel **C**), and average cells SV ratio of NPP (panel **D**).

example, temperature significantly correlated with abundance and biovolume of total NPP, chlorophytes, and cryptophytes but not with abundance of haptophytes or pedinellids. The differences existed also within taxonomic groups: abundance and biovolume of all haptophytes correlated only with DIN, but *Chrysochromulina* correlated also with SRP and *Haptolina* only with temperature (Supporting Information Table S3A,B). Similar differences were also observed for cell volume and SV ratios (Fig. 6C,D), e.g., cell size and SV ratio of haptophytes were best explained by temperature, SRP, and DIN, but of *Chrysochromulina* only by temperature (Supporting Information Table S3C,D). These results agree with my hypothesis and support the view that the observed different dynamics of studied algal groups could have resulted from temporal niche separation. However, it is important to realize that these are only correlative relationships that need to be verified experimentally.

Discussion

In this study, I obtained novel data on ecology of specific NPP groups: their diversity, abundance, biovolume, and cell size. The exploratory analysis of these data allowed for the insight into the factors that can potentially affect dynamics of these groups in coastal, brackish waters. As NPP tend to be a dominant fraction in terms of abundance, biovolume, and activity (Sherr et al. 2007; Piwosz et al. 2015*a*; Roy et al. 2017), such knowledge enhances the current understanding of processes within phytoplankton communities.

Phototrophic dinoflagellates and diatoms, which were not studied in detail here, might be important part of NPP (Kownacka et al. 2013). These groups have been intensively investigated in the Baltic Sea for over a century, and the collected knowledge on their temporal and spatial dynamics has allowed for development of diat/dino index for the assessment of environmental status (Wasmund et al. 2017). In contrast, the ecology of groups on which I focused here is less known, as they are either omitted (such as pelagophytes or pedinellids) or classified only at higher taxonomic resolution (e.g., cryptophytes) during routine phytoplankton surveys (Helcom 1988). As their contribution to total NPP abundance and biovolume is substantial (Figs. 2–3), it is important to fill this knowledge gap.

Coastal NPP communities are very dynamic, suggesting existence of temporal niche separation

The changes in nanoplankton diversity were very dynamic in the Gulf of Gdansk, with values of species richness and Shannon entropy varying over twofold from 1 week to another (Fig. 1B,C), but within a range reported previously (Piwosz et al. 2018). Such high dynamics points to the importance of temporal sampling in recovering the true picture of nanoplankton diversity on coastal waters.

Sequencing confirmed persistence of groups and phylotypes recovered previously from the Gulf of Gdańsk and the Baltic Sea (Hu et al. 2016; Piwosz et al. 2018). However, groups found abundant using CARD-FISH were under-represented in the sequencing libraries. Amplicon sequencing seems to be quantitatively inaccurate (Piwosz et al. 2015*b*; Grujčić et al. 2018) because of biases introduced during sample processing (Tedersoo et al. 2010). Therefore, I used the sequencing results mainly to select groups to be further analyzed by CARD-FISH.

Dynamics of heterotrophic nanoplankton abundance in coastal waters is very high (Piwosz and Pernthaler 2010; Piwosz and Pernthaler 2011). Here, I showed that this is also the case for the NPP, whose total abundance and biovolume varied up to 30-fold within a week (Figs. 2–3). A similar magnitude of weekly changes was observed at higher taxonomic levels, e.g., for chlorophytes, chrysophytes, or cryptophytes. However, at the level of order or genus, abundance and biovolume changed a 100-fold within a week, indicating their high growth and mortality rates and emphasizing their importance in food webs and biochemical cycling. Moreover, multiple peaks recovered at higher phylogenetic level were composed of distinct species or genera, as documented for cryptophytes, pedinellids, and haptophytes (Fig. 2B–D). This may be explained by temporal niche separation, possibly resulting from differences in their physiology which has been well documented for cultured *Prymnesium* and *Chrysochromulina* species (e.g., Jones et al. 1993; Hansen and Hjorth 2002; Graneli et al. 2012; Liu et al. 2015). The hypothesis of temporal niche separation was also supported by different correlations of studied algal groups with environmental variables (Fig. 6; Supporting Information Table S3), but such statistical analyses require experimental verification.

A seasonal pattern emerged from this high weekly dynamics, with some groups being more abundant in spring and other in summer or autumn (Figs. 2–3). Seasonal changes are well known in coastal waters for microphytoplanktonic diatoms and dinoflagellates (Aubry et al. 2004; Wasmund et al. 2011), but are poorly documented for specific nanophytoplanktonic groups. Unfortunately, a year's worth of data are insufficient to decipher existence of phenological phenomena. Summer maxima of haptophyte abundance, observed in the Gulf of Gdańsk in this study and in 2007 (Figs. 2–3; Supporting Information Fig. S7), were also observed in Skagerrak (Kuylenstierna and Karlson 1994; Lekve et al. 2006). Conversely, pedinellids showed their maxima in the Gulf of Gdańsk in October in 2012 (Fig. 2C) and in May/June in 2007 (Piwosz and Pernthaler 2010). A 2-yr-long series from eutrophic Rodrigo de Freitas Lagoon in Brazil showed lack of reccurent patterns for eustigmatophytes or cryptophytes (Alves-De-Souza et al. 2017). Multiannual time series are required to conclude on existence of recurrent phenological patterns of specific NPP groups (Stern et al. 2018).

NPP size structure in coastal waters

Size structure of phytoplankton communities is a fundamental feature for ecosystem functioning, as it determines primary production, nutrient cycling and export to deep waters, and food webs structure (Finkel et al. 2010). It is strongly affected by environmental factors, especially by concentration of nutrients, with larger cells predominating in eutrophic waters (Marañón 2015). Shifts in phytoplankton size structure typically result from shifts in the community composition (Marañón et al. 2012). However, whether and how cell size of specific species changes in the environment is less known, despite the fact that intraspecies cell size variability can be pronounced (Parke et al. 1955). Here, I showed that the cell volume and SV ratio varied substantially for all NPP and at class level, but they were rather invariable at genus, species, or a lineage level (Figs. 4–5). In contrast to my prediction, it was temperature that explained most of the variability in cell volume of the studied NPP groups in the Gulf of Gdańsk (Fig. 6C). As morphological diversity of nanophytoplanktonic algae is low compared to microalgal groups like diatoms and dinoflagellates, their SV ratio scales inversely (but not linearly) with cell volume. Still, the variability in SV ratios was most explained by SRP concentrations, whereas effect of temperature was almost two times lower (Fig. 6D). Moreover, different species may show various responses. For instance, cell volume of pedinellid species *A. radians* and *P. elastica* and of cryptophytes correlated stronger with concentrations of nutrients (DIN and SRP, respectively) than with temperature (Fig. 6; Supporting Information Table S3). Such variability between different species and groups emphasizes the complexity of processes controlling cell size of NPP species under natural conditions, where they are usually affected by multiple environmental factors at once (Browning et al. 2017).

Correlation studies do not allow causative understanding of relationships between the observed factors. Here, the measured environmental variables explained less than 50% of the observed variability in abundance, biovolume, cell size and SV ratio of the studied NPP groups, and remaining variability could likely have been explained by other factors, such as irradiance, grazing, or competition (Mei et al. 2009; Finkel et al. 2010; Marañón et al. 2013). For instance, abundance and biovolume of all studied groups and total NPP dropped almost to null during the massive bloom of *H. triquetra* (Figs. 2–3), and the only cells that could still be detected were large chlorophytes (average cell volume > 70 μm^3; Fig. 4C), indicating some sort of interspecies interactions but also a possible effect of high SRP concentration at that time (Supporting Information Fig. S4). Moreover, most studied groups are mixotrophic, which confounds their dependence on inorganic nutrients (Andersson et al. 1989; Jones et al. 1993; Tillmann 1998; Piwosz and Pernthaler 2010; Mckie-Krisberg and Sanders 2014; Grujčić et al. 2018). Finally, coastal waters are very dynamic systems, where plankton communities constantly mix (Bazin et al. 2014; Piwosz et al. 2018), affecting the observed dynamics in community composition and size structure of NPP. Experimental approaches are essential to verify whether the correlations observed here are meaningful, and to progress our understanding of NPP dynamics.

Conclusions

NPP dynamics in coastal waters of the Gulf of Gdańsk was very high, and abundance and biovolume of various NPP groups changed a 100-fold within a week. Studied algal groups showed distinct seasonal patterns and correlated differently with environmental variables, indicating temporal niche separation between closely related genera and species. Temporal changes in size volume and SV ratio were substantial at class level, but variability of cell size was low at genus/species level, indicating that the changes in NPP size structure resulted from changes in the community structure. Redundancy analysis pointed to concentration of DIN as the factor explaining most of the variability in the abundance and biovolume, to temperature for cell size, and to concentration of SRP for cell SV ratio. The importance of these correlation, and the possible mechanisms behind them, still need to be determined experimentally.

References

Alves-De-Souza, C., T. S. Benevides, J. B. O. Santos, P. Von Dassow, L. Guillou, and M. Menezes. 2017. Does environmental heterogeneity explain temporal β diversity of small eukaryotic phytoplankton? Example from a tropical eutrophic coastal lagoon. J. Plankton Res. **39**: 698–714. doi:10.1093/plankt/fbx026

Amann, R. I., B. J. Binder, R. J. Olson, S. W. Chisholm, R. Devereux, and D. A. Stahl. 1990. Combination of 16S ribosomal-RNA-targeted oligonucleotide probes with flow-cytometry for analyzing mixed microbial populations. Appl. Environ. Microbiol. **56**: 1919–1925.

Anderson, M. J., and P. Legendre. 1999. An empirical comparison of permutation methods for tests of partial regression coefficients in a linear model. J. Stat. Comput. Simul. **62**: 271–303. doi:10.1080/00949659908811936

Andersson, A., S. Falk, G. Samuelsson, and A. Hagstrom. 1989. Nutritional characteristics of a Mixotrophic Nanoflagellate, *Ochromonas* sp. Microb. Ecol. **17**: 251–262. doi:10.1007/BF02012838

Aubry, F. B., A. Berton, M. Bastianini, G. Socal, and F. Acri. 2004. Phytoplankton succession in a coastal area of the NW Adriatic, over a 10-year sampling period (1990-1999). Cont. Shelf Res. **24**: 97–115. doi:10.1016/j.csr.2003.09.007

Balzano, S., D. Marie, P. Gourvil, and D. Vaulot. 2012. Composition of the summer photosynthetic pico and nanoplankton communities in the Beaufort Sea assessed by T-RFLP and sequences of the 18S rRNA gene from flow cytometry sorted samples. ISME J. **6**: 1480–1498. doi:10.1038/ismej.2011.213

Bazin, P., F. Jouenne, A.-F. Deton-Cabanillas, A. Perez-Ruzafa, and B. Veron. 2014. Complex patterns in phytoplankton and microeukaryote diversity along the estuarine continuum. Hydrobiologia **726**: 155–178. doi:10.1007/s10750-013-1761-9

Browning, T. J., E. P. Achterberg, I. Rapp, A. Engel, E. M. Bertrand, A. Tagliabue, and C. M. Moore. 2017. Nutrient co-limitation at the boundary of an oceanic gyre. Nature **551**: 242–246. doi:10.1038/nature24063

Chao, A., K. H. Ma and T. C. Hsieh (2015). SpadeR: Species prediction and diversity estimation with R. R package version 0.1.0., [accessed on 2018 February 28]. Available from https://CRAN.R-project.org/package=SpadeR

Coleman, A. W. 1980. Enhanced detection of bacteria in natural environments by fluorochrone staining of DNA. Limnol. Oceanogr. **25**: 948–951. doi:10.4319/lo.1980.25.5.0948

De Vargas, C., and others. 2015. Eukaryotic plankton diversity in the sunlit ocean. Science **348**: 1261605. doi:10.1126/science.1261605

Edgar, R. C., B. J. Haas, J. C. Clemente, C. Quince, and R. Knight. 2011. UCHIME improves sensitivity and speed of chimera detection. Bioinformatics **27**: 2194–2200. doi:10.1093/bioinformatics/btr381

Edvardsen, B., W. Eikrem, J. Throndsen, A. G. Saez, I. Probert, and L. K. Medlin. 2011. Ribosomal DNA phylogenies and a morphological revision provide the basis for a revised taxonomy of the Prymnesiales (Haptophyta). Eur. J. Phycol. **46**: 202–228. doi:10.1080/09670262.2011.594095

Egge, E., L. Bittner, T. Andersen, S. Audic, C. De Vargas, and B. Edvardsen. 2013. 454 pyrosequencing to describe microbial eukaryotic community composition, diversity and relative abundance: A test for marine Haptophytes. PLoS One **8**: e74371. doi:10.1371/journal.pone.0074371

Egge, E. S., T. V. Johannessen, T. Andersen, W. Eikrem, L. Bittner, A. Larsen, R. A. Sandaa, and B. Edvardsen. 2015. Seasonal diversity and dynamics of haptophytes in the Skagerrak, Norway, explored by high-throughput sequencing. Mol. Ecol. **24**: 3026–3042. doi:10.1111/mec.13160

Eller, G., K. Toebe, and L. K. Medlin. 2007. Hierarchical probes at various taxonomic levels in the Haptophyta and a new division level probe for the Heterokonta. J. Plankton Res. **29**: 629–640. doi:10.1093/plankt/fbm045

Evans, C. A., J. E. O'reilly, and J. P. Thomas. 1987. A handbook for measurement of chlorophyll a and primary productivity. BIOMASS Science Series 8. Scientific Committee on Antarctic Research.

Finkel, Z. V., J. Beardall, K. J. Flynn, A. Quigg, T. a. V. Rees, and J. A. Raven. 2010. Phytoplankton in a changing world: Cell size and elemental stoichiometry. J. Plankton Res. **32**: 119–137. doi:10.1093/plankt/fbp098

Fuller, N. J., G. A. Tarran, D. G. Cummings, E. M. S. Woodward, K. M. Orcutt, M. Yallop, F. Le Gall, and D. J. Scanlan. 2006. Molecular analysis of photosynthetic picoeukaryote community structure along an Arabian Sea transect. Limnol. Oceanography **51**: 2502–2514. doi:10.4319/lo.2006.51.6.2502

Graneli, E., B. Edvardsen, D. L. Roelke, and J. A. Hagstrom. 2012. The ecophysiology and bloom dynamics of *Prymnesium* spp. Harmful Algae **14**: 260–270. doi:10.1016/j.hal.2011.10.024

Grasshoff, K., M. Ehrhardt, and K. Kremling. 1976. Methods for sea water analysis. Verlag Chemie.

Grujčić, V., J. K. Nuy, M. M. Salcher, T. Shabarova, V. Kasalicky, J. Boenigk, M. Jensen, and K. Simek. 2018. Cryptophyta as major bacterivores in freshwater summer plankton. ISME J. **12**: 1668–1681. doi:10.1038/s41396-018-0057-5

Guillou, L., and others. 2013. The Protist ribosomal reference database (PR2): A catalog of unicellular eukaryote small subunit rRNA sequences with curated taxonomy. Nucleic Acids Res. **41**: D597–D604. doi:10.1093/nar/gks1160

Hansen, P. J., and M. Hjorth. 2002. Growth and grazing responses of *Chrysochromulina ericina* (Prymnesiophyceae): The role of irradiance, prey concentration and pH. Mar. Biol. **141**: 975–983. doi:10.1007/s00227-002-0879-5

Helcom. 1988. Guidelines for the Baltic Monitoring Programme for the third stage. Baltic Sea Environmental Proceedings No. 27. Government Printing Centre.

Hu, Y. O. O., B. Karlson, S. Charvet, and A. F. Andersson. 2016. Diversity of Pico- to Mesoplankton along the 2000 km salinity gradient of the Baltic Sea. Front. Microbiol. **7**: 679. doi:10.3389/fmicb.2016.00679

Jones, H. L. J., B. S. C. Leadbeater, and J. C. Green. 1993. Mixotrophy in marine species of *Chrysochromulina* (Prymnesiophyceae)—ingestion and digestion of a small Green flagellate. J. Mar. Biol. Assoc. UK **73**: 283–296. doi:10.1017/S0025315400032859

Khanaychenko, A., V. Mukhanov, L. Aganesova, S. Besiktepe, and N. Gavrilova. 2018. Grazing and feeding selectivity of *Oithona davisae* in the Black Sea: Importance of Cryptophytes. Turkish J. Fish. Aquat. Sci. **18**: 937–949. doi:10.4194/1303-2712-v18_8_02

Kownacka, J., L. Edler, S. Gromisz, M. Łotocka, I. Olenina, M. Ostrowska, and K. Piwosz. 2013. Non-indigenous species *Chaetoceros cf. lorenzianus* Grunow 1863—a new, predominant component of autumn phytoplankton in the southern Baltic Sea. Estuar. Coast. Shelf Sci. **119**: 101–111. doi:10.1016/j.ecss.2013.01.010

Kuylenstierna, M., and B. Karlson. 1994. Seasonality and composition of pico- and nanoplanktonic cyanobacteria and protists in the skagerrak. Bot. Mar. **37**: 17–33. doi:10.1515/botm.1994.37.1.17

Legendre, P., and M. J. Anderson. 1999. Distance-based redundancy analysis: Testing multispecies responses in multifactorial ecological experiments. Ecol. Monogr. **69**: 1–24. doi:10.1890/0012-9615(1999)069[0001:DBRATM]2.0.CO;2

Lekve, K., E. Bagoien, E. Dahl, B. Edvardsen, M. Skogen, and N. C. Stenseth. 2006. Environmental forcing as a main determinant of bloom dynamics of the *Chrysochromulina* algae. Proc. R. Soc. B. Biol. Sci. **273**: 3047–3055. doi:10.1098/rspb.2006.3656

Lim, E. L., L. A. Amaral, D. A. Caron, and E. F. Delong. 1993. Application of ribosomal RNA-based probes for observing marine nanoplanktonic protists. Appl. Environ. Microbiol. **59**: 1647–1655.

Liu, Z., A. E. Koid, R. Terrado, V. Campbell, D. A. Caron, and K. B. Heidelberg. 2015. Changes in gene expression of *Prymnesium parvum* induced by nitrogen and phosphorus limitation. Front. Microbiol. **6**: 631. doi:10.3389/fmicb.2015.00631

Ludwig, W., and others. 2004. ARB: A software environment for sequence data. Nucleic Acids Res. **32**: 1363–1371. doi:10.1093/nar/gkh293

Marañón, E. 2015. Cell size as a key determinant of phytoplankton metabolism and community structure. Ann. Rev. Mar. Sci. **7**: 241–264. doi:10.1146/annurev-marine-010814-015955

Marañón, E., P. Cermeño, M. Latasa, and R. D. Tadonléké. 2012. Temperature, resources, and phytoplankton size structure in the ocean. Limnol. Oceanogr. **57**: 1266–1278. doi:10.4319/lo.2012.57.5.1266

Marañón, E., P. Cermeño, D. C. López-Sandoval, T. Rodríguez-Ramos, C. Sobrino, M. Huete-Ortega, J. M. Blanco, and J. Rodríguez. 2013. Unimodal size scaling of phytoplankton growth and the size dependence of nutrient uptake and use. Ecol. Lett. **16**: 371–379. doi:10.1111/ele.12052

Massana, R., R. Terrado, I. Forn, C. Lovejoy, and C. Pedros-Alio. 2006. Distribution and abundance of uncultured heterotrophic flagellates in the world oceans. Environ. Microbiol. **8**: 1515–1522. doi:10.1111/j.1462-2920.2006.01042.x

Mckie-Krisberg, Z. M., and R. W. Sanders. 2014. Phagotrophy by the picoeukaryotic green alga *Micromonas*: Implications for Arctic Oceans. ISME J. **8**: 1953–1961. doi:10.1038/ismej.2014.16

Mcmurdie, P. J., and S. Holmes. 2013. Phyloseq: An R package for reproducible interactive analysis and graphics of microbiome census data. PLoS One **8**: e61217. doi:10.1371/journal.pone.0061217

Medlin, L. K., A. G. Sáez, and J. R. Young. 2008. A molecular clock for coccolithophores and implications for selectivity of phytoplankton extinctions across the K/T boundary. Mar. Micropaleontol. **67**: 69–86. doi:10.1016/j.marmicro.2007.08.007

Mei, Z. P., Z. V. Finkel, and A. J. Irwin. 2009. Light and nutrient availability affect the size-scaling of growth in phytoplankton. J. Theor. Biol. **259**: 582–588. doi:10.1016/j.jtbi.2009.04.018

Metfies, K., and L. Medlin. 2007. Refining cryptophyte identification with DNA-microarrays. J. Plankton Res. **29**: 1071–1075. doi:10.1093/plankt/fbm080

Monchy, S., and others. 2012. Microplanktonic community structure in a coastal system relative to a *Phaeocystis* bloom inferred from morphological and tag pyrosequencing methods. PLoS One **7**: e39924. doi:10.1371/journal.pone.0039924

Morison, F., and S. Menden-Deuer. 2018. Seasonal similarity in rates of protistan herbivory in fjords along the Western Antarctic Peninsula. Limnol. Oceanogr. **63**: 2858–2876. doi:10.1002/lno.11014

Oksanen, J., and others. 2018. vegan: Community ecology package. R package version 2.4-6. [accessed on 2018 February 28]. Available from https://cran.r-project.org/package=vegan.

Olenina, I., and others. 2006. Biovolumes and size-classes of phytoplankton in the Baltic Sea. HELCOM Baltic Sea Environ. Proc. **106**: 144.

Parke, M., I. Manton, and B. Clarke. 1955. Studies on marine flagellates II. Three new species of *Chrysochromulina*. J. Mar. Biol. Assoc. UK **34**: 579–609. doi:10.1017/S0025315400008833

Pinckney, J. L., C. R. Benitez-Nelson, R. C. Thunell, F. Muller-Karger, L. Lorenzoni, L. Troccoli, and RamonVarela. 2015. Phytoplankton community structure and depth distribution changes in the Cariaco Basin between 1996 and 2010. Deep-Sea Res. Part I-Oceanogr. Res. Pap. **101**: 27–37. doi:10.1016/j.dsr.2015.03.004

Piwosz, K., and J. Pernthaler. 2010. Seasonal population dynamics and trophic role of planktonic nanoflagellates in coastal surface waters of the southern Baltic Sea. Environ. Microbiol. **12**: 364–377. doi:10.1111/j.1462-2920.2009.02074.x

Piwosz, K., and J. Pernthaler. 2011. Enrichment of omnivorous Cercozoan nanoflagellates from coastal Baltic Sea waters. PLoS One **6**: e24415. doi:10.1371/journal.pone.0024415

Piwosz, K., K. Spich, J. Całkiewicz, A. Weydmann, A. M. Kubiszyn, and J. M. Wiktor. 2015*a*. Distribution of small phytoflagellates along an Arctic fjord transect. Environ. Microbiol. **17**: 2393–2406. doi:10.1111/1462-2920.12705

Piwosz, K., J. Villiger, and J. Pernthaler. 2015*b*. Numbers vs. reads: Comparison of patterns in algal dynamics revealed by high throughput sequencing and microscopic counts. Eur. J. Phycol. **50**: 134–134.

Piwosz, K., J. Kownacka, A. Ameryk, M. Zalewski, and J. Pernthaler. 2016. Phenology of cryptomonads and the CRY1 lineage in a coastal brackish lagoon (Vistula Lagoon, Baltic Sea). J. Phycol. **52**: 626–637. doi:10.1111/jpy.12424

Piwosz, K., J. Całkiewicz, M. Gołębiewski, and S. Creer. 2018. Diversity and community composition of pico- and nanoplanktonic protists in the Vistula River estuary (Gulf of Gdańsk, Baltic Sea). Estuar. Coast. Shelf Sci. **207**: 242–249. doi:10.1016/j.ecss.2018.04.013

Quince, C., A. Lanzen, R. J. Davenport, and P. J. Turnbaugh. 2011. Removing noise from pyrosequenced amplicons. BMC Bioinformatics **12**: 38. doi:10.1186/1471-2105-12-38

R Core Team 2015. R: A language and environment for statistical computing. R Foundation for Statistical Computing. Vienna, Austria: http://www.R-project.org/.

Roy, S., S. Sathyendranath, and T. Platt. 2017. Size-partitioned phytoplankton carbon and carbon-to-chlorophyll ratio from ocean colour by an absorption-based bio-optical algorithm. Remote Sens. Environ. **194**: 177–189. doi:10.1016/j.rse.2017.02.015

Sekiguchi, H., M. Kawachi, T. Nakayama, and I. Inouye. 2003. A taxonomic re-evaluation of the Pedinellales (Dictyochophyceae), based on morphological, behavioural and molecular data. Phycologia **42**: 165–182. doi:10.2216/i0031-8884-42-2-165.1

Shabarova, T., J. Villiger, O. Morenkov, J. Niggemann, T. Dittmar, and J. Pernthaler. 2014. Bacterial community structure and dissolved organic matter in repeatedly flooded subsurface karst water pools. FEMS Microbiol. Ecol. **89**: 111–126. doi:10.1111/1574-6941.12339

Shalchian-Tabrizi, K., J. Brate, R. Logares, D. Klaveness, C. Berney, and K. S. Jakobsen. 2008. Diversification of unicellular eukaryotes: Cryptomonad colonization of marine and fresh waters inferred from revised 18S rRNA phylogeny. Environ. Microbiol. **10**: 2635–2644. doi:10.1111/j.1462-2920.2008.01685.x

Sherr, B. F., E. B. Sherr, and R. D. Fallon. 1987. Use of monodispersed, fluorescently labeled bacteria to estimate in situ protozoan bacterivory. Appl. Environ. Microbiol. **53**: 958–965.

Sherr, B. F., B. F. Sherr, D. A. Caron, D. Vaulot, and A. Z. Worden. 2007. Oceanic protists. Oceanography **20**: 130–134. doi:10.5670/oceanog.2007.57

Simon, N., J. Brenner, B. Edvardsen, and L. K. Medlin. 1997. The identification of *Chrysochromulina* and *Prymnesium* species (Haptophyta, Prymnesiophyceae) using fluorescent or chemiluminescent oligonucleotide probes: A means for improving studies on toxic algae. Eur. J. Phycol. **32**: 393–401. doi:10.1080/09670269710001737339

Simon, N., L. Campbell, E. Ornolfsdottir, R. Groben, L. Guillou, M. Lange, and L. K. Medlin. 2000. Oligonucleotide probes for the identification of three algal groups by dot blot and fluorescent whole-cell hybridization. J. Eukaryot. Microbiol. **47**: 76–84. doi:10.1111/j.1550-7408.2000.tb00014.x

Stamatakis, A., P. Hoover, and J. Rougemont. 2008. A rapid bootstrap algorithm for the RAxML web-servers. Syst. Biol. **75**: 758–771. doi:10.1080/10635150802429642

Stefanidou, N., S. Genitsaris, J. Lopez-Bautista, U. Sommer, and M. Moustaka-Gouni. 2018. Unicellular eukaryotic community response to temperature and salinity variation in Mesocosm experiments. Front. Microbiol. **9**: 2444. doi:10.3389/fmicb.2018.02444

Stern, R., and others. 2018. Molecular analyses of protists in long-term observation programmes—current status and future perspectives. J. Plankton Res. **40**: 519–536. doi:10.1093/plankt/fby035

Stoeck, T., D. Bass, M. Nebel, R. Christen, M. D. Jones, H. W. Breiner, and T. A. Richards. 2010. Multiple marker parallel tag environmental DNA sequencing reveals a highly complex eukaryotic community in marine anoxic water. Mol. Ecol. **19**: 21–31. doi:10.1111/j.1365-294X.2009.04480.x

Tedersoo, L., and others. 2010. 454 pyrosequencing and sanger sequencing of tropical mycorrhizal fungi provide similar results but reveal substantial methodological biases. New Phytol. **188**: 291–301. doi:10.1111/j.1469-8137.2010.03373.x

Tillmann, U. 1998. Phagotrophy by a plastidic haptophyte, *Prymnesium patelliferum*. Aquat. Microb. Ecol. **14**: 155–160. doi:10.3354/ame014155

Wasmund, N., J. Tuimala, S. Suikkanen, L. Vandepitte, and A. Kraberg. 2011. Long-term trends in phytoplankton composition in the western and Central Baltic Sea. J. Mar. Syst. **87**: 145–159. doi:10.1016/j.jmarsys.2011.03.010

Wasmund, N., J. Kownacka, J. Göbel, A. Jaanus, M. Johansen, I. Jurgensone, S. Lehtinen, and M. Powilleit. 2017. The diatom/Dinoflagellate index as an indicator of ecosystem changes in the Baltic Sea 1. Principle and handling instruction. Front. Mar. Sci. **4**: 22. doi:10.3389/fmars.2017.00022

Wickham, H. 2009. ggplot2: Elegant graphics for data analysis. Springer-Verlag.

Wilke, C. O. 2018. cowplot: Streamlined plot theme and plot annotations for 'ggplot2'. R package version 0.9.3, [accessed on 2018 Feb 28]. Available from https://CRAN.R-project.org/package=cowplot

Yilmaz, L. S., S. Parnerkar, and D. R. Noguera. 2011. mathFISH, a web tool that uses thermodynamics-based mathematical models for in Silico evaluation of oligonucleotide probes for fluorescence in situ hybridization. Appl. Environ. Microbiol. **77**: 1118–1122. doi:10.1128/AEM.01733-10

Acknowledgments

I would like to thank my colleagues from the National Marine Fisheries Research Institute (Poland): Gosia Kownacka for help with samples collection, Mariusz Zalewski for analysis of Chl *a*, and Hanna Wróblewska for analysis of nutrients. I would also like to thank Jörg Villiger and Jakob Pernthaler from the University of Zurich for processing the sequence data. Finally, Jason Dean from the Center Algatech Institute of Microbiology Czech Academy of Sciences was kind and patient enough to correct the language. The study was supported by the Czech Ministry of Education project Algatech Plus (LO1416).

Conflict of Interest

None declared.

Submitted 14 September 2018
Revised 07 February 2019
Accepted 20 March 2019

Associate editor: Maren Voss